Self-consistent electronic structure of surfaces: Surface states and surface resonances on W(001)

M. Posternak* and H. Krakauer
Department of Physics and Astronomy, Northwestern University, Evanston, Illinois 60201

A. J. Freeman
Department of Physics and Astronomy, Northwestern University, Evanston, Illinois 60201 and Argonne National Laboratory, Argonne, Illinois 60439

D. D. Koelling
Argonne National Laboratory, Argonne, Illinois 60439

(Received 14 January 1980)

Surface states (SS) and surface resonances (SR) on the W(001) surface have been determined from the first self-consistent energy-band study of this metal surface. The calculations were performed for a seven-layer film using our thin-film linearized augmented-plane-wave method which includes all relativistic corrections except the spin-orbit interaction. Self-consistency was found to be essential for obtaining an accurate value of the work function -4.5 ± 0.2 eV, in excellent agreement with experiment. No evidence was found for surface core-level shifts as observed in photoemission from the (110) surface, indicating the possible importance of final-state effects. A complete description of all three experimentally observed resonance bands is given for the first time: SS and SR states are found to exist in different portions of the two-dimensional Brillouin zone; their location and symmetry are in very good agreement with structure observed in photoemission at 0.3, 0.8, and 4.2 eV below the Fermi energy, E_F. Particularly interesting is the close agreement of the never before obtained $\vec{k}_{\parallel}=0$ true SS (at -0.3 eV) with experiment.

I. INTRODUCTION

The last few years have witnessed a dramatic increase in experimental and theoretical studies of transition-metal surfaces. Electronic states which are localized near the surface are among the most prominent of the observed spectroscopic features. Experimentally, however, there is often little difference between surface states (SS), which decay exponentially into the bulk, and surface resonances (SR), which can be described as a hybrid of a true surface state and a bulk state. If SS and SR are relatively well understood on semiconductor and simple metal surfaces,[1] it is only relatively recently that attempts have been made to deal with the additional complexity arising from d electrons in noble and transition metals. So far, self-consistent calculations have been performed for only a few surfaces of $3d$ metals [Sc (Ref. 2), Ti (Ref. 3), Fe (Ref. 4), Ni (Ref. 5), Cu (Ref. 6)] and $4d$ metals [Nb (Ref. 7), Mo (Ref. 8), Pd (Ref. 9), Ag (Ref. 10)], but not for any of the $5d$ metal surfaces. However, the most extensively studied metallic surface resonances occur on the W(001) surface,[11–16] and the origin and nature of these states has been a long standing problem. The wealth of detailed experimental information on W(001), reviewed below, thus presents a well charted area in which to explore the theory of surface electronic structure.

An "anomalous" peak in the W(001) field-emission energy distribution (FEED) was first discovered by Swanson and Crouser,[12] and a similar feature was subsequently observed on the (001) face of Mo.[13] The W(001) peak was originally interpreted in terms of the relativistic bulk band structure,[12] but a later FEED study by Plummer and Gadzuk[14] identified it as a surface state. The state on W(001) was also reported as the first observation of a metallic surface state using photoemission.[15] Weng *et al.*[16] have recently presented a very complete review of the SS and SR on the (001) surfaces of Mo and W, utilizing both angle-resolved photoemission (ARP) and FEED. They concluded that many-body effects (e.g., final-state relaxation, plasma interaction) and d-band edge effects are not required to explain any aspect of the photoemission results from these resonances. Experimentally, then, three bands of surface resonances are observed in the ARP experiments[16] on W(001): (i) A high-lying SR is located 0.3 eV below the Fermi energy, E_F. The intensity of this resonance peaks at normal exit ($\vec{k}_{\parallel}=0$) and decreases rapidly as $|\vec{k}_{\parallel}|$ increases (off-normal emission). This state has even parity with respect to mirror plane

symmetry (e.g., d_{z^2} or s-orbital character). (ii) For emission angles greater than 2° an additional second high-lying resonance appears as a shoulder about 0.8 eV below the first high-lying resonance. Its photoemission intensity is strictly zero at normal exit ($\vec{k}_{\parallel}=0$), but increases gradually with increasing polar angle reaching a maximum at around 10° ($|\vec{k}_{\parallel}| \simeq 0.2$ to 0.3 Å^{-1}). Weng *et al.*[16] suggest that this resonance has odd parity with respect to a (110) mirror plane although they note evidence that it may contain a small component of even parity. (iii) The third band is similar to the first but is located about 4.2 eV below E_F. Experimentally the dispersion is less than 0.3 eV for each band.

The theoretical interpretation of these spectroscopic features [especially the first high-lying band (i)] in terms of initial-state properties of surface states and surface resonance states has been quite controversial. Feder and Sturm[17] found a SR in a "relative" or filled spin-orbit gap at $\vec{k}=(0,0)$ near E_F as well as a true SS in a spin-orbit symmetry gap just below the "relative gap." Both of these states have Δ_7 symmetry, however, and Hermanson[18] showed that this was not consistent with the ARP observations of Feuerbacher and Fitton[19] for the high-lying resonance band. Kasowski[20] found a SS of the correct symmetry in the vicinity of E_F at $k_{\parallel}=0$, but only for a contracted surface. [It has since been suggested,[16] however, that this state be identified with the low-lying (4.2 eV) resonance at $\vec{k}_{\parallel}=0$.] Noguera *et al.*[21] also required a surface contraction (for Mo) to obtain a SS at $\vec{k}_{\parallel}=0$ near E_F. Modinos and Nicolaou,[22] by contrast, interpreted the high-lying resonance (i) as being due to SR states near E_F which they found for finite $\vec{k}_{\parallel}\neq 0$ (i.e., near $\vec{k}_{\parallel}=0$ but not strictly at $\vec{k}_{\parallel}=0$). Similar results have been obtained by other non-self-consistent calculations,[16,23–28] but comparison with the most recent experimental results leads to the conclusion[16] that while these calculations can be interpreted as correctly predicting both the existence and symmetry of the second high-lying resonance (ii) and the low-lying resonance (iii), they fail to explain the first high-lying resonance. (Inglesfield's[29] calculation yields an unoccupied SS state near E_F at $\vec{k}_{\parallel}=0$; this result, however, is in contradiction with the experimental observation that this state exists below E_F.) This somewhat unusual situation is explained by the fact that the existence of the high-lying surface resonance is very sensitive to the potential near the surface, as discussed in Sec. III. Indeed, Kerker *et al.*[8] demonstrated that self-consistency was required in order to get an occupied high-lying resonance at $\vec{k}_{\parallel}=0$ for Mo(001) as well as the other resonances (ii) and (iii). However, Kerker *et al.*[8] show only the second high-lying resonance along the $\bar{\Gamma}\bar{M}$ direction, in contradiction to the experimental observation of all three bands. This may be due to their use of a film with only five layers.

In this paper, we present the first self-consistent band-structure calculation for the W(001) surface using a previously described[30] thin-film energy-band method based on the bulk linearized-augmented-plane-wave (LAPW) method.[31] The calculations were performed for a seven-layer film and include all relativistic corrections except the spin-orbit interaction. These calculations provide, for the first time, a complete description of all three experimentally observed resonance bands. Self-consistency also was found to be essential in obtaining accurate work function results: our value (4.5 ± 0.2) eV is in excellent agreement with the experimental value of 4.63 eV.[32] In addition, we do not find any core-level shift of the surface atoms relative to bulk, in agreement with the predictions of a very simple model for the origin of such shifts.

The paper is organized as follows: Sec. II outlines the self-consistent film LAPW method of calculation; Sec. III presents our results, compares them with available experimental data, and briefly discusses the possible role of some of these resonance states on the $c(2\times 2)$ reconstruction of W(001); and Sec. IV summarizes our principle conclusions. Finally, technical aspects of solving Poisson's equation are presented in the Appendix.

II. METHOD OF CALCULATION

The film band-structure calculations are performed using the previously described film LAPW method.[30] The modifications for including self-consistency and treating more general potentials are described below.

A slight redefinition of the basis function in the interstitial region has also been implemented: as before[30] the basis function in the interstitial region (region II in Fig. 1) is defined as a product of a two-dimensional plane-wave and a one-dimensional symmetrized plane-wave appropriate for films with z-reflection symmetry

$$\phi_{m,n}(\vec{k},\vec{r}) = (2/\Omega)^{1/2}\exp[i(\vec{k}+\vec{g}_m)\cdot\vec{r}] \times \begin{cases} \cos(k_n z); & (+) \\ \sin(k_n z); & (-) \end{cases} \quad (1)$$

Here (+) and (−) denote states which are, respectively, symmetric and antisymmetric with respect to z reflection; $\vec{k}$ is a two-dimensional crystal momentum vector, $\vec{g}_m$ is a two-dimensional reciprocal-lattice vector, and Ω equals the volume of the unit cell between $z=\pm\frac{1}{2}D$ where D is the distance between boundary planes touching the two outermost muffin-tin (MT) spheres as in Fig. 1. Unlike Ref. 30, k_n is defined in terms of the distance D' with $D'>D$

$$k_n \equiv \begin{cases} n2\pi/D'; & (+) \\ (n+\frac{1}{2})2\pi/D'; & (-), \quad n=0,1,2,3,\ldots . \end{cases} \quad (2)$$

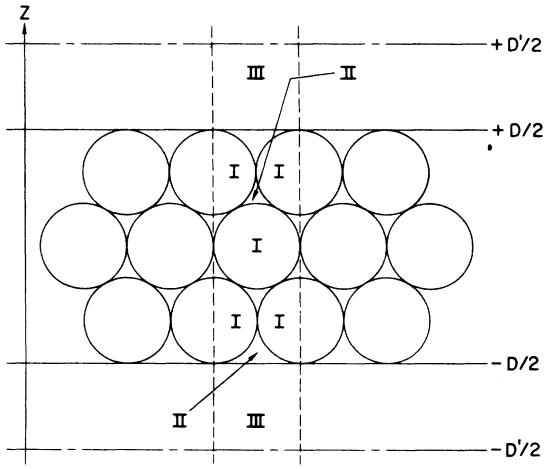

FIG. 1. Schematic representation of the film muffin-tin (FMT) potential. The unit cell, indicated by dashed lines, extends to $z = \pm\infty$. Region I denotes the muffin-tin spheres, region II denotes the interstitial, and region III ($|z| > \frac{1}{2}D$) denotes the vacuum region. The representation of the LAPW basis function in the interstitial region (II) involves a one-dimensional Fourier expansion over the interval $-\frac{1}{2}D' \leq z \leq \frac{1}{2}D'$.

Simply put, the fictitious periodic boundary conditions used to make the basis set discrete are no longer required to coincide with our partitioning of space. There is no reason to do so since it actually creates artificial problems by unduly restricting the basis set.[30] Now the first derivative, ∂/∂_z, of the basis function is no longer restricted to be identically zero at the planar boundaries ($z = \pm\frac{1}{2}D$) [see the discussion after Eq. (2) in Ref. 30]. The value of $D' = D + 2R_{\mathrm{MT}}$ is used in the calculation, where R_{MT} is the bulk muffin-tin (MT) radius. Since the seven-layer bcc W(001) slab has z-reflection symmetry, the LAPW basis is otherwise constructed exactly as before.[30] We have not included a contraction of the surface interlayer spacing,[33] and all seven MT radii in the unit cell were set equal to the maximum possible bulk MT radius, $R_{\mathrm{MT}} = \frac{1}{4}a\sqrt{3}$, where a is the bulk lattice parameter (5.793 a.u.).

A. Full potential in the interstitial and vacuum regions

The film muffin-tin (FMT) potential is used to construct the film LAPW basis functions. In the vacuum ($|z| > \frac{1}{2}D$ in Fig. 1), this potential depends only on the z coordinate, i.e., $V_{\mathrm{FMT}}(z)$ is the planar average of the full potential in vacuum $V^{\mathrm{vac}}(\vec{r})$. Inside the planar boundaries of the film ($|z| \leq \frac{1}{2}D$ in Fig. 1), this potential is spherically symmetric in the MT spheres centered on the nuclear sites and $V_{\mathrm{FMT}} = \bar{V}' = \text{const}$ in the interstitial region, i.e., $V_{\mathrm{FMT}}(|\vec{r}|)$ is the spherical average of the full potential, $V(\vec{r})$ in the MT spheres and $\bar{V}' = \text{const}$ is the volume average of the full potential in the interstitial region [the zero of energy is usually adjusted so that $\bar{V}' = 0$]. Once defined, however, this basis can be used to treat the full potential $V(\vec{r})$ without any shape approximation, since the film LAPW secular equations are obtained through application of the Rayleigh-Ritz variational principle. The full Hamiltonian matrix is then given by Eq. (7) of Ref. 30

$$H = H_{\mathrm{FMT}} + \Delta H_{I,V} + \Delta H_{\mathrm{NS}} \ , \tag{3}$$

where H_{FMT} is due to the FMT potential, $\Delta H_{I,V}$ is due to the non-FMT correction potential in the interstitial region, and in the vacuum region, and ΔH_{NS} is due to the nonspherical correction potential in the MT spheres. In the present calculation, we have included $\Delta H_{I,V}$ but have neglected ΔH_{NS}. (In bulk calculations, the use of spherically averaged potentials inside the MT spheres and the full potential in the interstitial regions is known as the warped muffin-tin approximation and appears to be an excellent approximation for metals.) Thus, in the present calculation the full potential is treated everywhere except inside the MT spheres.

In order to obtain the correction term in the interstitial region, ΔH_I (where $\Delta H_{I,V} = \Delta H_I + \Delta H_V$) we define the potential $\tilde{V}^I(\vec{r})$

$$\tilde{V}^I(\vec{r}) = \begin{cases} V^I(\vec{r}); & \vec{r} \in \text{interstitial} \ , \\ 0, & \text{elsewhere} \ . \end{cases} \tag{4}$$

$\tilde{V}^I(\vec{r})$ can be expanded in a plane-wave star representation,[34]

$$\tilde{V}^I(\vec{r}) = \sum_{n,s} \tilde{V}^I_{n,s} \cos(k_n z) \phi_s(\vec{r}) \ , \tag{5a}$$

where the two-dimensional (2D) star function $\phi_s(\vec{r})$ has the full 2D symmetry of the film and is given by

$$\phi_s(\vec{r}) = \frac{1}{n_0} \sum_R e^{i\hat{R}\vec{G}_s \cdot (\vec{r} - \vec{t}_R)} \ . \tag{5b}$$

Here $\vec{G}_s$ is a 2D star representative reciprocal-lattice vector, $\hat{R}$ is the point group part of 2D space-group operation, R, $\vec{t}_R$ is a nonprimitive 2D translation vector, and n_0 is the number of 2D space-group operations. For the unreconstructed W(001) film considered here, there are eight 2D space-group operations, and all the $\vec{t}_R$ can be set to zero since the space group is symmorphic. Inspection of the form of the film LAPW basis function in the interstitial region [Eq. (1) of Ref. 30] shows that the matrix elements of ΔH_I, $\langle n'm' | \tilde{V}^I(\vec{r}) | nm \rangle$, are trivially related to the Fourier components, $\tilde{V}^I_{n,s}$, in Eq. (5a).

The correction term in vacuum, ΔH_V, is obtained similarly from the vacuum 2D star expansion

$$V^{\mathrm{vac}}(\vec{r}) = \sum_s V^{\mathrm{vac}}_s(z) \phi_s(\vec{r}) \ . \tag{6}$$

Note that the FMT potential in the vacuum region, $V_{\rm FMT}(z)$, is simply equal to $V_{s=0}^{\rm vac}(z)$. Inspection of Eq. (4a) in Ref. 30 then shows that the matrix elements of ΔH_V, $\langle n'm'|[V^{\rm vac}(\vec{r}) - V_{\rm FMT}(z)]|nm\rangle$, are simply determined by one-dimensional z integrals involving the functions $V_s^{\rm vac}(z)$ [Eq. (6)] and the z-dependent functions $u_{\vec{k},m}(E_v,z)$ and $\dot{u}_{\vec{k},m}(E_v,z)$ [Eq. (4a) in Ref. 30], where $u(E_v,z)$ is a solution of the one-dimensional Schrödinger equation in the vacuum region [Eq. (4b) in Ref. 30] and $\dot{u}(E_v,z)$ is its energy derivative.

As we are performing a local density function theory[35] calculation, the potential is expressed as a sum of the Coulomb and exchange-correlation potentials

$$V(\vec{r}) = V_{\rm Coul}(\vec{r}) + V_{\rm xc}(\vec{r}) \ . \tag{7}$$

The Fourier star-representations [Eqs. (5a) and (6)] for $V_{\rm Coul}(\vec{r})$ are obtained from the charge density $\rho(\vec{r})$ by solving Poisson's equation, as described in the Appendix. Given the form of the LAPW basis functions in the interstitial and vacuum regions, it is completely straightforward to obtain expressions for $\rho(\vec{r})$ similar to Eqs. (5a) and (6), and, solving Poisson's equation, one obtains $V_{\rm Coul}(\vec{r})$ in the desired representations. $V_{\rm xc}(\vec{r})$ (see below) is a nonlinear function of $\rho(\vec{r})$, however, so we have followed Koelling *et al.*[34] in obtaining the star representation of $V_{\rm xc}^I(\vec{r})$ by performing a least-squares Fourier fit in the interstitial region. Using a sampling of about 1000 $\vec{r}$ points in the interstitial, we obtain fits such that the rms error is about 0.1% of the average value of $V^{\rm xc}(\vec{r})$ in the interstitial. We find $V_{s,\rm xc}^{\rm vac}(z)$ [Eq. (6)] in a similar manner by performing least-squares two-dimensional Fourier fits in each of the i planes for which $V_s^{\rm vac}(z_i)$ is tabulated. ($V_{s=\phi}^{\rm vac}$ is tabulated on a linear mesh out to 20 a.u. from the planar boundaries, but $V_{s\neq\phi}^{\rm vac}$ is tabulated on the same linear mesh only out to 10 a.u. from the planar boundaries, because the latter coefficients fall off to zero much more rapidly than does $V_{s=0}^{\rm vac}$.)

B. Self-consistent procedure

In local density functional theory, the exchange and correlation potential is given by

$$V^{\rm xc}(n(\vec{r})) = \frac{d}{dn}[n\epsilon_{\rm xc}(n)] \ , \tag{8}$$

where $n(\vec{r})$ is the electronic density and $\epsilon_{\rm xc}(n)$ is the exchange and correlation energy per particle of the uniform electron gas. We have taken $\epsilon_{\rm xc}$ to be that given by the Wigner interpolation formula[36]

$$\epsilon_{\rm xc}(n) = -[0.916/r_s + 0.88/(r_s+7.8)] \ {\rm Ry} \ , \tag{9a}$$

with a spatially dependent r_s defined by

$$\tfrac{4}{3}\pi r_s^3(\vec{r}) \equiv [n(\vec{r})]^{-1} \ , \tag{9b}$$

where $n(\vec{r})$ is the total electron density.

The starting potential was constructed from overlapping atomic charge densities with the atomic configuration for W taken to be (Xe) $4f^{14}5d^56s^1$. As detailed in Ref. 30, the radial functions in the MT spheres are obtained by solving the Dirac equation using a method developed by Koelling and Harmon[37] which includes all relativistic kinematic effects, but drops the spin-orbit interaction. In each iteration the core charge density [(Xe)$4f^{14}$] is recomputed using the film muffin-tin potential in a fully relativistic (i.e., including spin-orbit) Dirac-Slater-type atomic structure program (using the Wigner interpolation formula for $V_{\rm xc}$). In the initial iterations, eigenvalues and eigenvectors are calculated at three special points[38] in the irreducible $\frac{1}{8}$ of the two-dimensional square BZ pictured in Fig. 2. In the final iterations a ten-point set of special points[38] is used, and in the last iteration a uniform 15 k-point set is used. The symmetrized basis size was about 210 LAPW's which corresponds to about 60 LAPW's per atom. The resulting eigenvalues are converged to better than about 3 mRy. From the total charge density, $\rho_{\rm total} = \rho_{\rm valence} + \rho_{\rm core}$, a new film potential is generated. The new potential is mixed with the current input potential to obtain the input potential for the next iteration (10% of the new potential is the largest mixing). We consider self-consistency achieved when the maximum difference between the input potential and the output potential is less than about 0.2 eV. The eigenvalues are converged to better than 3 mRy well before the potential is converged for the next iteration.

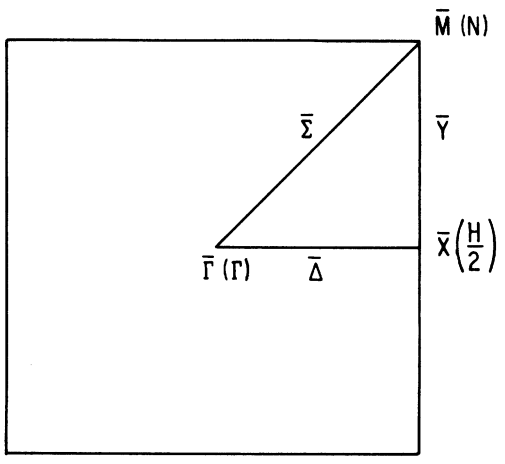

FIG. 2. Irreducible $\frac{1}{8}$ of the two-dimensional square Brillouin zone for the bcc (001) surface. If the two-dimensional square Brillouin zone is oriented to pass through the center of the three-dimensional bcc Brillouin zone, the $\bar{M}$ point coincides with the bulk symmetry point N, and the $\bar{X}$ point is located on the bulk Δ symmetry line half-way to H along a [010] or [100] direction.

Omitting the spin-orbit coupling[37] requires approximating the $j = l + \frac{1}{2}$ and $j = l - \frac{1}{2}$ radial function by an average radial function. (For W this is a more severe approximation than assuming the energy dependence of the radial basis function to be linear.) To assess the importance of this j-averaging approximation, we have compared results of self-consistent calculations on bulk W using the spin-orbit omitted LAPW approach with those obtained from the fully relativistic APW (RAPW) method. We find that the core charge density is unaffected to five significant figures. (This is not surprising as in both calculations it was determined with the full Dirac radial equation and the indirect effects of the conduction electrons due to spin orbit only should be minimal.) The density at the muffin-tin sphere boundary—where conduction-electron effects dominate—agreed to 0.05% with a very slight (0.02 electron) movement of charge out of the muffin-tin spheres.

III. RESULTS

The self-consistent solution of the film LAPW equations yields eigenvalues and eigenfunctions which may be used to derive a variety of theoretical results. Our major objective is to obtain information about the effect of the surface by comparison with experiment and, in particular, with those experimental results described earlier.

A. Charge density and work function

Since the charge density is of fundamental importance in local density functional theory, we examine first the total self-consistent charge density and the resulting work function as this is a sensitive test of the quality of the results obtained. Figure 3 shows the total valence charge density, $\rho(\vec{r})$ (i.e., the core charge density has been subtracted) in a (110) plane for positive z values. Nonspherical components of $\rho(\vec{r})$ inside the muffin-tin spheres were constructed using the angular momentum representation of the LAPW wave functions [Eq. (3) in Ref. 30] retaining all contributions up to $l_{max} = 6$ in the wave functions (in the SC iterations $l_{max} = 8$). The resulting nonspherical charge-density components are truncated at a maximum value of $l = 8$. The unretouched $\rho(\vec{r})$ pictured in Fig. 3 exhibits minimal discontinuities across the sphere boundaries, which shows that satisfactory l convergence in $\rho(\vec{r})$ has been obtained. The charge density is seen to fall off smoothly as one progresses normal to the surface into the vacuum and to very rapidly "heal" to bulklike character on going away from the surface into the solid. Each layer of the film is approximately charge neutral (including the vacuum charge as part of the surface layer).

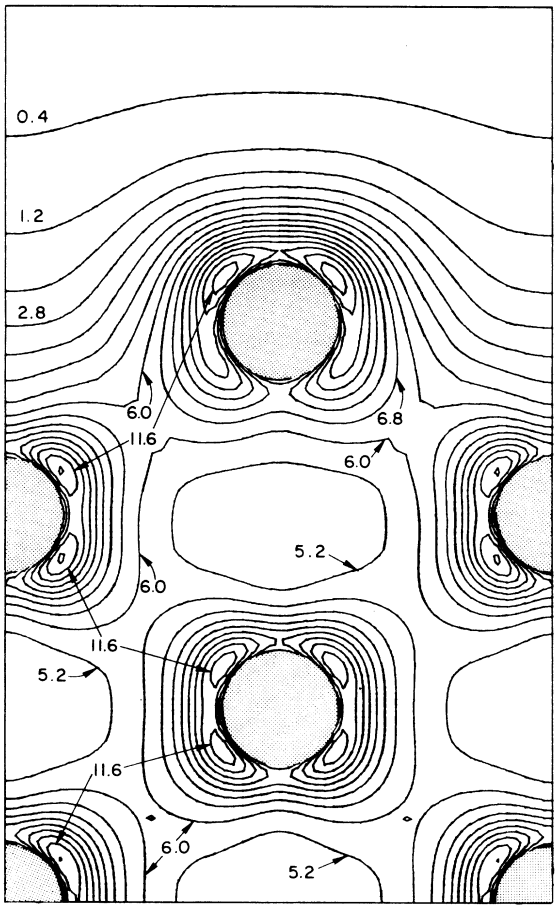

FIG. 3. Contour plot of the total valence charge density. Successive contours are separated by 0.8 in units of electrons per bulk unit cell.

The bonding characteristics are also evident in Fig. 3. In the interior atoms, the bonding xy,xz,yz (t_{2g}) d orbitals form fairly localized lobes pointing along the body diagonals to the nearest-neighbor atoms. In addition, there is a rather uniform metallic bonding charge density in the interstitial regions. These features persist up to the second layer from the surface. In the surface layer, there are marked changes in the bonding character. Compared to an interior atom, substantial weight has been removed from the lobes pointing towards the missing nearest neighbor above the film, although the maximum value of the d-band charge density is still about the same in these directions. By contrast, the maximum value in the downward pointing lobes is somewhat reduced as a consequence of an increased charge transfer into this bond from the surface atom. Finally, there is a large and rapid variation in $\rho(r)$ in the interstitial region of the surface layer, demonstrating the importance of the "warping" contributions to the potential.

There is a sizeable redistribution of charge near the

surface associated with the formation of the dipole layer, which sensitively determines the work function. As expected, self-consistency is found to be crucial for obtaining an accurate value of the work function, ϕ. We find $\phi = 4.5 \pm 0.2$ eV (the uncertainty reflecting the degree of self-consistency obtained in the potential), in excellent agreement with experiment.[32]

B. Layer density of states

Since most of the eigenvalue information plotted as band structure is complex and not easily assimilated (in such plots the 3D bulk band structure is essentially projected onto the 2D Brillouin zone which tends to obscure details about surface states as well as the underlying bulk bands), we focus first on the information contained in the theoretical layer by layer density of states (DOS). The local density of states (LDOS) for each layer, shown in Fig. 4, was obtained using the two-dimensional analog[5] of the bulk linear analytic tetrahedron method.[39] [The LDOS shown

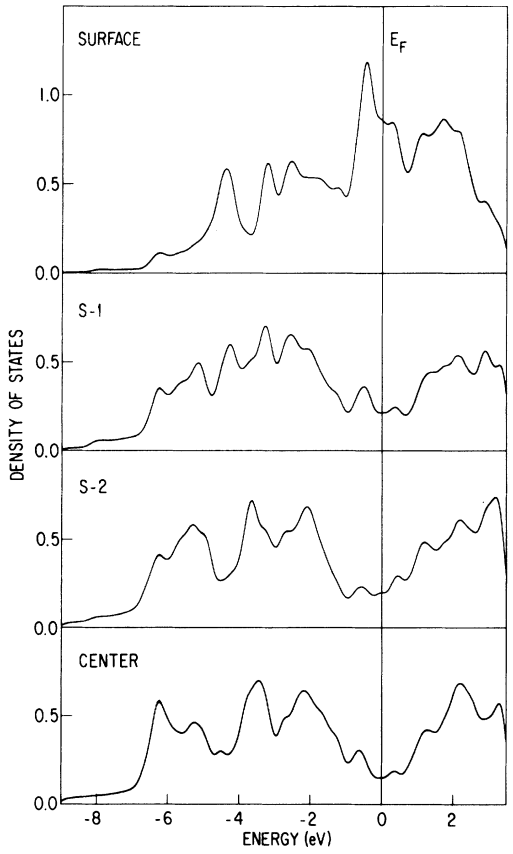

FIG. 4. Layer projected density of states for the seven-layer film. S-1 is the first layer in from the surface and S-2 is the second layer in from the surface.

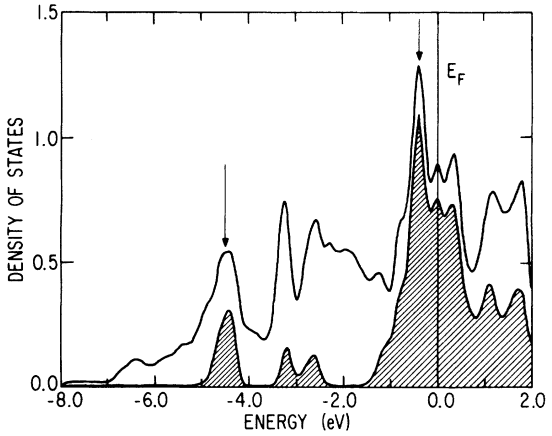

FIG. 5. Layer projected density of states for the surface layer. The shaded region represents the (positive) excess density of states in the surface layer over the central layer.

were obtained using 15 $\vec{k}$ points in the irreducible $\frac{1}{8}$ of the two-dimensional BZ and then smoothed with a Gaussian (FWHM = 0.3 eV).] The general trend seen is that of an approach to bulk behavior in going from the surface to the central layer, since the latter, indeed, displays the characteristic structure of the tungsten bulk DOS. The bandwidth is already achieved by the second layer. There are two prominent peaks in the surface LDOS (Fig. 5) indicated by arrows at -0.5 and -4.4 eV. To better understand their origin we show, as shaded regions, the excess surface DOS (surface minus central layer; positive values only). This way of plotting the results indicates the possible SS or SR origin of these peaks. As we will show shortly, the one located at about 0.5 eV below the Fermi energy is related partly to a short SS line of states around $\bar{\Gamma}(\vec{k} \approx 0)$ and partly to a double SR line of states for $\vec{k} > 0$; the second, located at -4.4 eV, corresponds to a low-lying SR band. These resonances are found in both angle-integrated and angle-resolved photoemission.[16]

C. Surface states and surface resonances

In order to obtain information about SS and SR we display in Fig. 6, along the high-symmetry directions, those SS and SR which have a localization greater than 70% in the two outermost layers. For ease of reference, the bottom of the conduction band is shown along the lower portion of the figure. An analysis of these results shows that they provide for the first time good agreement with detailed ARP measurements[16] of all three surface resonance bands described in the Introduction.

(i) There is an extremely localized state just below E_F near $\bar{\Gamma}$ which has a small upwards dispersion along

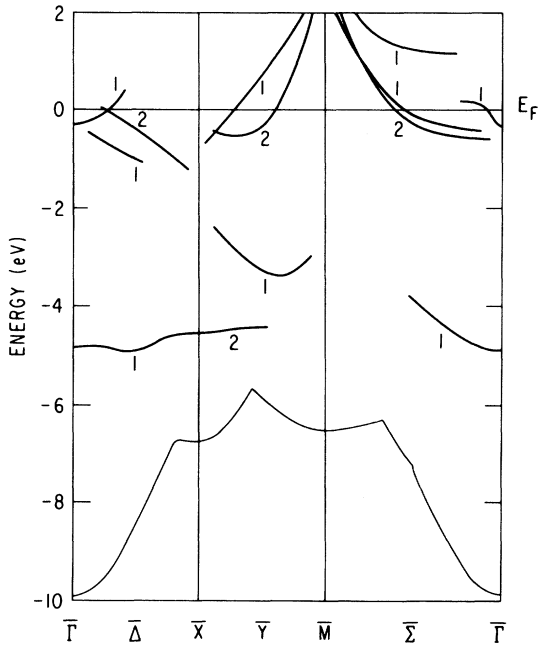

FIG. 6. Surface states and resonances with a localization greater than 70% in the two outermost layers of the film. The bottom of the conduction band is outlined along the lower portion of the figure.

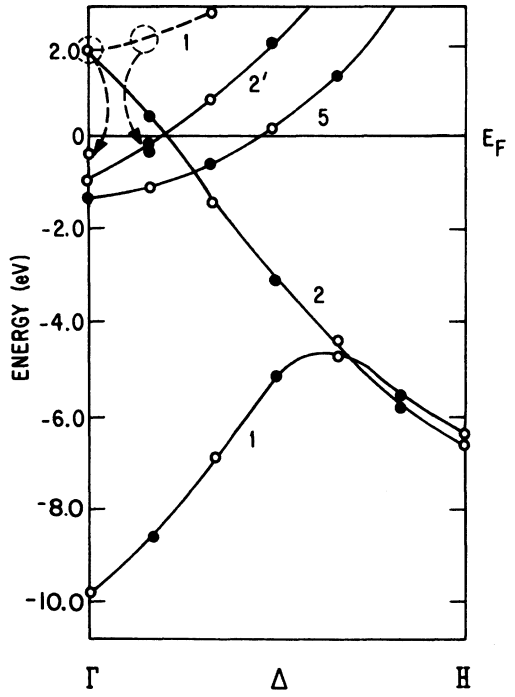

FIG. 7. Film-derived "bulk" energy bands along ΓH, showing the origin of the very localized surface state 0.3 eV below E_F at $\bar{\Gamma}(\vec{k}_{\parallel}=0)$.

$\bar{\Gamma}\bar{X}$ and $\bar{\Gamma}\bar{M}$ with $\bar{\Delta}_1$ and $\bar{\Sigma}_1$ symmetry in agreement with experiment. It disappears about one-third of the way between $\bar{\Gamma}\bar{X}$ and $\bar{\Gamma}\bar{M}$. This is the state which is seen as a sharp peak in photoemission spectra at normal exit. It is a true SS only at $\bar{\Gamma}$ where it exists in a bulk $\bar{\Delta}_1$ symmetry gap.

Figure 7 shows the origin of the surface state at $\bar{\Gamma}$. We have displayed all of the film energy eigenvalues at $\bar{\Gamma}$ as though they were derived from the projection of the three-dimensional cyrstal band structure along ΓH in the bulk bcc Brillouin zone (open circles are even and solid circles are odd with respect to z reflection). The general shape of the bulk bands along ΓH is recognized, and we note the near degeneracy of the film $\Delta_{2'}$ and Δ_5 bands at Γ, reflecting the exact degeneracy of the bulk bands at the $\Gamma_{25'}$ point. (The lower symmetry due to the presence of the surface does not require this degeneracy.) Similarly, the film Δ_1 and Δ_2 bands are nearly degenerate at H, reflecting the exact degeneracy of the bulk bands at the H_{12} point. This is a further indication that the seven-layer film quite adequately reproduces the bulk as well as the surface band structure. This figure shows that two states from the upper Δ_1 branch are shifted downwards into a Δ_1 symmetry gap, giving rise to the pair of SS odd and even with respect to z reflection. As mentioned, this SS is very sensitive to the actual potential. Our starting potential, for example, does not yield this SS. These results confirm early predictions by Caruthers and Kleinman[40] for SS at $\bar{\Gamma}$ on transition-metal bcc (001) surfaces. In calculations for Fe(001), they found that both the existence and symmetry of SS at $\bar{\Gamma}$ depend crucially on details of the potential and are very dependent on small changes in the potential. On the W(001) surface studied here, the $\bar{\Gamma}_1$ SS just below E_F is extremely localized in the surface layer ($\sim 93\%$) and projects quite far out into the vacuum region (see Fig. 8). Thus, it is perhaps not surprising that the conditions for the formation of this state are sensitive to the behavior of the potential near the surface. The surface potential in turn depends on the delicate rearrangement of electronic charge at the surface which leads to the formation of the surface dipole barrier and the correct work function. The treatment of this electronic screening is, of course, beyond the scope of non-self-consistent calculations, and it explains the general failure of such calculations to predict correctly the high-lying $\bar{\Gamma}_1$ SS.

(ii) We also find a *pair* of SR (for $\vec{k}_{\parallel}\neq 0$) about 0.5 eV below the SS described above. Along the symmetry lines $\bar{\Gamma}\bar{X}$ and $\bar{\Gamma}\bar{M}$, one of the pair of SR is symmetric ($\bar{\Delta}_1$ and $\bar{\Sigma}_1$, respectively) and the other is antisymmetric ($\bar{\Delta}_2$ and $\bar{\Sigma}_2$, respectively) with respect to the corresponding mirror planes [a (100) plane

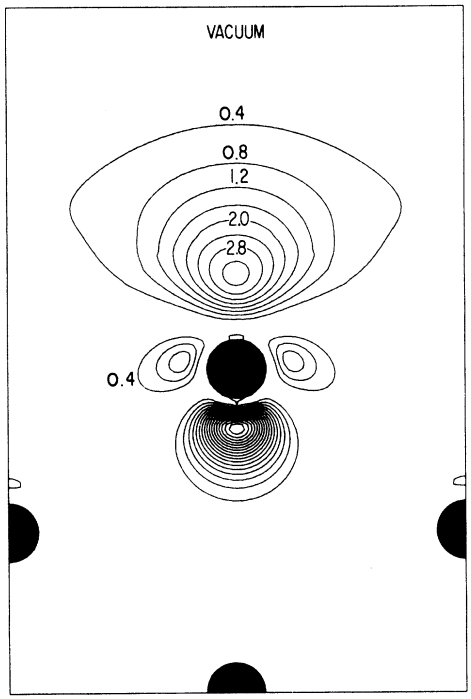

FIG. 8. Charge-density contour plot for the very localized surface state 0.3 eV below E_F at $\bar{\Gamma}(\vec{k}_{\parallel}=0)$. Successive contours are separated by 0.4 in units of electrons per bulk unit cell.

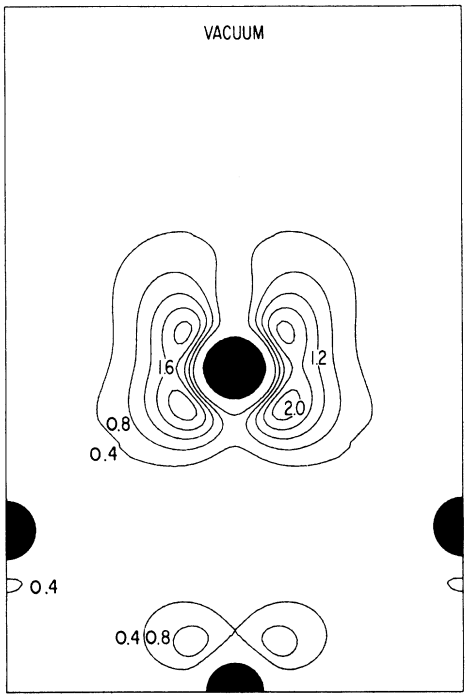

FIG. 9. Charge density for the $\bar{\Sigma}_1$ surface resonance near E_F at $\vec{k}_{\parallel}=(0.5,0.5)\pi/a$. Successive contours are separated by 0.4 in units of electrons per bulk unit cell.

along $\bar{\Gamma}\bar{X}$ and a (110) plane along $\bar{\Gamma}\bar{M}$]. Along the $\bar{\Gamma}\bar{M}$ direction these states have a small upward dispersion (in agreement with experiment) cutting E_F about half-way between $\bar{\Gamma}$ and $\bar{M}$. Along the $\bar{\Gamma}\bar{X}$ direction, however, these states have a small downward dispersion (similar dispersion was found along $\bar{\Gamma}\bar{X}$ in a self-consistent calculation[8] for Mo), whereas the experimentally determined dispersion[16] is slightly upward toward E_F. We do not believe that this is a size effect due to the use of a five-layer film in Ref. 8 or our use of a seven-layer film, since Grise *et al.*[28] found a slight *upward* dispersion along $\bar{\Gamma}\bar{X}$ of their $\bar{\Delta}_1$ SR state for both five- and seven-layer films as well as for a 39-layer film.

It is important to note that the $\bar{\Sigma}_2$ SR is about 20–25% more localized in the two outermost layers than is the $\bar{\Sigma}_1$ SR (below E_F, the localization in the topmost two layers is typically greater than 90% for the $\bar{\Sigma}_2$ SR). Contour plots for the $\bar{\Sigma}_1$ and $\bar{\Sigma}_2$ SR are shown in Figs. 9 and 10, respectively. Taken together with the fact that the $\bar{\Sigma}_1$ and $\bar{\Sigma}_2$ SR have nearly the same energy and dispersion, this could explain the weak shoulder found in Fig. 9 of Weng *et al.*[16] when the vector potential $\vec{A}$ is parallel to $\vec{k}$ along $\bar{\Gamma}\bar{M}$. The presence of this shoulder led Weng *et al.* to suggest that this SR might possibly contain a small com-

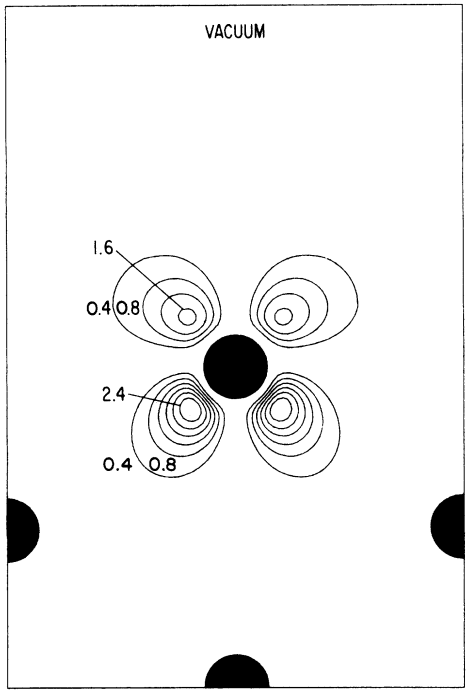

FIG. 10. Charge density for the $\bar{\Sigma}_2$ surface resonance near E_F at $\vec{k}_{\parallel}=(0.5,0.5)\pi/a$. Successive contours are separated by 0.4 in units of electrons per bulk unit cell.

ponent of even ($\bar{\Sigma}_1$) parity, although the predominant component seemed to be of odd ($\bar{\Sigma}_2$) parity. The results of our calculation show that the $\bar{\Sigma}_1$ SR is less localized than the $\bar{\Sigma}_2$ SR and would thus be expected to give a smaller contribution to the photoemission intensity. Grise *et al.*[28] invoked spin-orbit coupling to explain this observation. Whereas they find only a single SR with odd parity ($\bar{\Sigma}_2$) when spin-orbit coupling is neglected, the inclusion of spin-orbit coupling shows that this state acquires a small component of even-parity. By contrast, we find *two* SR, one of each parity, without resorting to the spin-orbit interaction.

(iii) Finally, there is a low-lying SR with very flat dispersion along $\bar{\Gamma}\bar{X}$ and part of the way along $\bar{X}\bar{M}$ at about -4.5 eV. This state is also found part of the way along $\bar{\Gamma}\bar{M}$, but is much less localized and shows a greater dispersion. The symmetries are, respectively, $\bar{\Delta}_1$, $\bar{Y}_2$, and $\bar{\Sigma}_1$, in agreement with the experimentally determined ($\bar{\Delta}_1\bar{\Sigma}_1$) low-lying resonance. This SR band corresponds to the low-lying peak in the surface LDOS seen in Fig. 5.

In addition to these three bands of SR which have been experimentally observed, we find additional SR, which are pictured in Fig. 6. The low-lying $\bar{\Delta}_1$ SR at about -4.5 eV continues as a $\bar{Y}_2$ SR fading away about half-way between $\bar{X}\bar{M}$. To our knowledge, this $\bar{Y}_2$ SR has not yet been observed. Just above this state, there is a $\bar{Y}_1$ SR. Near E_F, there is another pair of SR, one of which is symmetric ($\bar{Y}_1$) and one of which is antisymmetric ($\bar{Y}_2$) with respect to the (010) mirror plane. Along $\bar{\Gamma}\bar{M}$ there is an unoccupied SR with $\bar{\Sigma}_1$ symmetry which comes down to within about 1 eV of E_F.

It is instructive to analyze and discuss the nature of these SS and SR in more detail. To do this, we display in Figs. 8–10 charge-density contour plots of some SS and SR in a $(1\bar{1}0)$ vertical plane. Figure 8 shows the charge density of the SS at $\bar{\Gamma}$, just below the Fermi energy. It projects quite far into the vacuum region and is directed to the missing second-nearest neighbor. The state has $d_{3z^2-r^2}$ character, and as mentioned earlier, it is precisely this state which is probed by photoemission experiments at normal exit. This feature is believed[16] to be similar to one occurring for Mo(001). The similarity of our Fig. 8 and Fig. 2 of Ref. 8, confirms this interpretation. The theoretical explanation of the origin and nature of this feature (the so-called Swanson[12,13] hump) can, therefore, now be considered to be finally settled. Figures 9 and 10 show the two resonances Σ_1 and Σ_2, respectively, computed at $\vec{k} = (\frac{1}{2}, \frac{1}{2})\pi/a$ (actually the sum over the star of this $\vec{k}$ vector). The $\bar{\Sigma}_1$ state (Fig. 9) has largely xy and $(xz + yz)$ orbital character, while the $\bar{\Sigma}_2$ state has $(x^2 - y^2)$ and $(xz - yz)$ orbital character. We note that the principal orbital content of these states is the same as that found by Smith and Mattheiss[24] along $\bar{\Gamma}\bar{M}$. By contrast, Grise *et al.*[28] find only the $\bar{\Sigma}_2$ state near $\bar{\Gamma}$.

D. Generalized susceptibility and surface phase transition

The SC band-structure results have been used[41] to compute the electronic generalized susceptibility function including matrix elements and local-field corrections for the W(001) surface. This function, which represents the response of the system to a periodic perturbation with wave vector $\vec{q}$, displays a sharp peak at $\bar{M}$ (due to 2D Fermi-surface nesting of the $\bar{\Sigma}_1$ and $\bar{\Sigma}_2$ states) which is compatible with the observed $c(2\times 2)$ reconstruction[42] of this surface. These results suggest the possibility that electronic surface-resonance states near the Fermi energy drive the phase transition through a surface phonon softening and gapping of the 2D Fermi surface, in agreement with a model proposed by Tosatti.[43]

E. Core-level shifts

Recently, the $4f$ levels at the surface of W(110) were reported to shift by about 0.3 eV to lower binding energies.[44] As mentioned above, in our work the core levels are recalculated in each iteration using the fully relativistic solution of the Dirac-Slater equation. We did not find *any* core-level shift for the surface atom in our calculation, in agreement with the prediction of a simple model[45] for core-level shifts. According to this model if the Fermi energy falls above the center of the d band, one would expect a shift to lower binding energies, as has been found experimentally for Au (0.4 eV).[45] On the other hand, for a less than half-filled d band, the model predicts a shift to greater binding energies. Thus shifts to greater binding energies of 0.22 and 0.48 eV for Ti[3] and Sc[2] were predicted by recent self-consistent film calculations. For W with five $5d$ electrons, the model thus predicts no shift relative to bulk atoms. As a check, we also calculated the $4f$ levels as *band* eigenvalues. There is no significant dispersion of these bands, and the eigenvalues are equal to the j-averaged value of the fully relativistic eigenvalues. Again we find no core-level shift. Our result is not dependent, therefore, on details of the method of calculation for the core states. Final-state many-body relaxation effects may, of course, contribute to measured core-level shifts. These can be roughly divided into intraatomic and interatomic contributions. Because of the high density of partially occupied surface resonances on W(001) (Figs. 4–6), the interatomic contributions at the surface may not be the same as those for a bulk atom and this effect may contribute to measured surface core-level shifts. Any such contributions could be in addition to those due to differences of local en-

vironment and coordination numbers between bulk and surface atom.

IV. CONCLUSION

In summary, we have presented the first self-consistent semirelativistic calculation of the tungsten (001) surface. We have found that SS and SR states exist in different portions of the two-dimensional BZ. Their location and symmetry are in good agreement with the structure observed in various photoemission experiments at 0.3, 0.8, and 4.2 eV below E_F. In particular, the $\vec{k}_{\parallel}=0$ true SS at -0.3 eV, which is in agreement with photoemission results, has not been obtained in any previous calculation.

Our calculations, as well as those performed earlier, were for the unreconstructed W(001) surface. Experimentally[42] it has been found that as the temperature is lowered below about 300 K a sharp low-energy-electron diffraction (LEED) pattern of $(\frac{1}{2},\frac{1}{2})$ spots emerges which is characteristic of this phase. This transformation seems to be of second order and is reversible on varying only the temperature. There is evidence, however, that the clean W(001) surface is already in the $c(2\times 2)$ reconstructed phase even at room temperature, where very diffuse $(\frac{1}{2},\frac{1}{2})$ LEED spots are observed.[46] Recent ion-scattering results[47] also indicate that the surface W atoms are displaced from their (1×1) positions. The precise nature of the transformation and the atomic displacements is not known and to date no detailed models have been proposed which explain both the LEED and ion-scattering data.[47] Calculations for the unreconstructed surface can be used, however, to investigate possible electronic contributions to the phase transition. Indeed, the calculated resonance states cutting the Fermi energy at midpoint between $\bar{\Gamma}$ and $\bar{M}$ have been used[41] to support a charge-density wave interpretation of the observed reconstruction of the W(001) surface. Further, since the photoemission experiments were performed at room temperature, the good agreement between our calculation and experiment suggests that the SS and SR states are not very sensitive to the displacements of the atoms at room temperature, where the $(\frac{1}{2},\frac{1}{2})$ LEED spots are diffuse. Thus, it would be interesting to study the behavior of the surface resonances as the temperature is lowered to where the $c(2\times 2)$ LEED pattern is sharp.

The theoretical work function, $\phi=4.5\pm 0.2$ eV was found to be in excellent agreement with experiment.[32] No evidence was found for surface core-level shifts as observed in photoemission for the W(110) surface, suggesting the possible importance of final-state effects omitted from this ground-state calculation. We note, finallly, that the good agreement for both the SS and SR was obtained without invoking an interlayer contraction of the surface plane, indicating that the results obtained are also not sensitive to this contraction. Calculations for the contracted W(001) surface are in progress.

ACKNOWLEDGMENTS

We are pleased to acknowledge helpful discussions with W. Pickett. This work was supported in part by the U.S. NSF (Grant No. DMR 77-23776 and through the Northwestern University Materials Research Center Grant No. DMR 76-80847), the U.S. DOE, and The Swiss National Science Foundation.

APPENDIX: SOLUTION OF POISSON'S EQUATION

The total charge density in this calculation has the following representation:

$$\rho(\vec{r})=\begin{cases}\rho^{\text{atom}}(|\vec{r}_\alpha|)=\rho_\alpha(|\vec{r}_\alpha|)-2Z_\alpha\delta(\vec{r}_\alpha), \\ \qquad\qquad |\vec{r}_\alpha|\le R_\alpha\ , \\ \rho^{I}(\vec{r})=\sum_{n,s}\rho^{I}_{n,s}\cos(k_n z)\phi_s(\vec{r}), \\ \qquad\qquad \vec{r}\in \text{interstitial}\ , \\ \rho^{\text{vac}}(\vec{r})=\sum_{s}\rho^{\text{vac}}_{s}(z)\phi_s(\vec{r}), \\ \qquad\qquad |z|\ge \frac{1}{2}D(\text{vacuum})\ ,\end{cases} \tag{A1}$$

where $\vec{r}_\alpha\equiv\vec{r}-\vec{\tau}_\alpha$ and $\vec{\tau}_\alpha$ is the position of the αth MT sphere. In Eq. (A1), $\rho_\alpha(|\vec{r}_\alpha|)$ is the spherically averaged total electronic charge density, Z_α is the nuclear charge, R_α is the radius of the αth MT sphere, and $\phi_s(\vec{r})$ is a 2D plane-wave star function [Eq. (3a)]. It is convenient to express $\rho(\vec{r})$ still in a dual representation but not space restricted within the film (i.e., $|Z|\le\frac{1}{2}D$). Besides the restriction in the present calculation for having a spherical charge density inside the MT spheres, this dual representation is obtained following the procedure outlined by Elyashar and Koelling.[48] First, the plane-wave representation in the interstitial, $\rho^I(\vec{r})$, is continued into the MT spheres, and the spherical average of $\rho^I(\vec{r})$ [denoted by $\rho^I(|\vec{r}|)$] is subtracted from $\rho^{\text{atom}}(\vec{r})$ inside the spheres. Second, a neutralizing Gaussian density, $g_\alpha(|\vec{r}_\alpha|)\equiv(\epsilon_\alpha^3/\pi^{3/2})Q_\alpha\exp(-\epsilon_\alpha^2 r_\alpha^2)$, is added to each MT sphere, and its Fourier transform is subtracted from the plane-wave representation of $\rho(\vec{r})$. Here Q_α is chosen to yield a neutral charge density inside the MT spheres, and ϵ is chosen such that $g_\alpha(\vec{r}_\alpha)$ can be approximated as lying entirely inside the MT sphere. In this form, the dual representation for the total charge density inside the film is given by the sum of an atomiclike term and a

nearly-free-electron (NFE)-like term

$$\rho(\vec{r}) = \tilde{\rho}^{\text{atom}}(\vec{r}) + \rho^{\text{NFE}}(\vec{r}); \quad |z| \leq \tfrac{1}{2}D \quad , \tag{A2a}$$

where

$$\tilde{\rho}^{\text{atom}}(\vec{r}) = \sum_{\alpha}[\rho_{\alpha}(|\vec{r}_{\alpha}|) - 2Z_{\alpha}\delta(\vec{r}_{\alpha}) - \rho'(|\vec{r}|) + g_{\alpha}(|\vec{r}|)] \tag{A2b}$$

and

$$\rho^{\text{NFE}}(\vec{r}) = \rho'(\vec{r}) - \sum_{\alpha} g_{\alpha}(|\vec{r} - \vec{\tau}_{\alpha}|), \quad |z| \leq \tfrac{1}{2}D \quad ,$$
$$= \sum_{n,s}(\rho^{I}_{n,s} - g_{n,s})\cos(k_n z)\phi_s(\vec{r}), \quad |z| \leq \tfrac{1}{2}D \quad . \tag{A2c}$$

In Eq. (A2c), $g_{n,s}$ is the Fourier expansion coefficient for $\sum_{\alpha} g_{\alpha}(|\vec{r}_{\alpha}|)$. Since the integral of $\tilde{\rho}^{\text{atom}}(\vec{r})$ is zero by construction, $\tilde{\rho}^{\text{atom}}(\vec{r})$ does not contribute to the Coulomb potential *anywhere* outside of the MT spheres. Thus, the total Coulomb potential outside the MT spheres depends only on $\rho^{\text{NFE}}(\vec{r})$ and $\rho^{\text{vac}}(\vec{r})$. Inside the MT spheres, the total (spherically averaged) Coulomb potential is given by standard expressions involving radial integrals of $\tilde{\rho}^{\text{atom}}(\vec{r})$ plus the spherical average of the potential due to $[\rho^{\text{NFE}}(\vec{r}) + \rho^{\text{vac}}(\vec{r})]$.

The potential due to $\rho'(\vec{r}) = [\rho^{\text{NFE}}(\vec{r}) + \rho^{\text{vac}}(\vec{r})]$ is determined as follows. Write

$$\rho'(\vec{r}) = \sum_{s}\rho'_s(z)\phi_s(\vec{r}) \quad , \tag{A3a}$$

where

$$\rho'_s(z) \equiv \begin{cases} \sum_{n}(\rho^{I}_{n,s} - g_{n,s})\cos(k_n z), & |z| \leq \tfrac{1}{2}D \quad , \\ \rho^{\text{vac}}_s(z), & |z| \geq \tfrac{1}{2}D \quad . \end{cases} \tag{A3b}$$

The Coulomb potential due to $\rho'(\vec{r})$ can then also be expressed as

$$V'(\vec{r}) = \sum_{s} V'_s(z)\phi_s(\vec{r}) \quad . \tag{A4}$$

Following Appelbaum and Hamann,[49] we substitute Eqs. (A3a) and (A4) into Poisson's equation to yield:

$$\left(g_s^2 - \frac{d^2}{dz^2}\right)V'_s(z) = 4\pi\rho'_s(z) \quad . \tag{A5}$$

We solve Eq. (A5) in a manner similar to that described in Ref. 49 and thus obtain $V'_s(z)$. Because $\rho^{\text{NFE}}(\vec{r})$ has a simple plane-wave representation inside the film, contributions to the potential due to $\rho^{\text{NFE}}(\vec{r})$ can be determined analytically, while contributions due to $\rho^{\text{vac}}_s(z)$ can be obtained numerically as in Ref. 49.

*Now at the EPFL, Laboratoire de Physique Appliquée, CH-1003 Lausanne, Switzerland.

[1]J. A. Appelbaum and D. R. Hamann, Rev. Mod. Phys. 48, 479 (1976).

[2]P. J. Feibelman and D. R. Hamann, Solid State Commun. 31, 413 (1979).

[3]P. J. Feibelman, J. A. Appelbaum, and D. R. Hamann, Phys. Rev. B 20, 1433 (1979). Also see Ref. 2.

[4]C. S. Wang and A. J. Freeman (unpublished).

[5]C. S. Wang and A. J. Freeman, Phys. Rev. B 19, 793 (1979); B 19, 4930 (1979); B (to be published); O. Jepsen and O. K. Andersen (unpublished).

[6]J. G. Gay, J. R. Smith, and F. J. Arlinghaus, Phys. Rev. Lett. 38, 561 (1977); 42, 332 (1979); J. A. Appelbaum and D. R. Hamann, Solid State Commun. 27, 881 (1978).

[7]S. G. Louie, K. M. Ho, J. R. Chelikowski, and M. L. Cohen, Phys. Rev. Lett. 37, 1289 (1976); Phys. Rev. B 15, 5627 (1977).

[8]G. P. Kerker, K. M. Ho, and M. L. Cohen, Phys. Rev. Lett. 110, 1593 (1978); G. P. Kerker, M. T. Yin, and M. L. Cohen, Solid State Commun. 32, 433 (1979).

[9]S. G. Louie, Phys. Rev. Lett. 40, 1525 (1978); 42, 476 (1979).

[10]J. A. Appelbaum and D. R. Hamann in Ref. 6.

[11]B. Feuerbacher and R. F. Willis, J. Phys. C 9, 169 (1976), and references therein.

[12]L. W. Swanson and L. C. Crouser, Phys. Rev. Lett. 16, 389 (1966).

[13]L. W. Swanson and L. C. Crouser, Phys. Rev. Lett. 19, 1179 (1967).

[14]E. W. Plummer and J. W. Gadzuk, Phys. Rev. Lett. 25, 1493 (1970).

[15]B. J. Waclawski, and E. W. Plummer, Phys. Rev. Lett. 29, 783 (1972); B. Feuerbacher and B. Fitton, *ibid.* 29, 786 (1972).

[16]Shang-Lin Weng, E. W. Plummer, and T. Gustafsson, Phys. Rev. B 18, 1718 (1978), and references therein.

[17]R. Feder and K. Sturm, Phys. Rev. B 12, 537 (1975).

[18]J. Hermanson, Solid State Commun. 22, 9 (1977).

[19]B. Feuerbacher and B. Fitton, Solid State Commun. 15, 295 (1974).

[20]R. V. Kasowski, Solid State Commun. 17, 179 (1975).

[21]C. Noguera, D. Spanjaard, D. Jepsen, Y. Ballu, C. Guillot, J. Lecante, J. Paigne, Y. Petroff, R. Pinchaux, P. Thiry, and R. Conti, Phys. Rev. Lett. 38, 1171 (1977).

[22]A. Modinos and N. Nicolaou, Phys. Rev. B 13, 1536 (1976).

[23]N. Kar and P. Soven, Solid State Commun. 20, 977 (1976).

[24]N. V. Smith and L. F. Mattheiss, Phys. Rev. Lett. 37, 1494 (1976).

[25]M. C. Desjonqueres and F. Cyrot-Lackman, J. Phys. F 6, 567 (1976).

[26]O. Bisi, C. Calandra, P. Flaviani, and F. Manghi, Solid State Commun. 21, 121 (1977).

[27]B. Laks and C. F. T. Goncalves da Silva, Solid State Commun. 25, 401 (1978).

[28]W. R. Grise, D. G. Dempsey, L. Kleinman, and K. Mednick, Phys. Rev. B 20, 3045 (1979).
[29]J. E. Inglesfield, Surf. Sci. 76, 379 (1978).
[30]H. Krakauer, M. Posternak, and A. J. Freeman, Phys. Rev. B 19, 1706 (1979).
[31]O. K. Andersen, Phys. Rev. B 12, 3060 (1975); D. D. Koelling and G. O. Arbman, J. Phys. F 5, 2041 (1975).
[32]R. L. Billington and T. N. Rhodin, Phys. Rev. Lett. 41, 1602 (1978).
[33]For a recent review of LEED intensity analysis of a possible surface contraction, see M. N. Reed and G. J. Russell, Surf. Sci. 88, 95 (1979). They conclude that due to uncertainties in the theoretical and experimental LEED profiles, the surface layer contraction cannot be ascertained. High-energy ion-scattering experiments on W(001) set an upper limit on the contraction of 6%: I. Stensgaard, L. C. Feldman, and P. J. Silverman, Phys. Rev. Lett. 42, 247 (1979); L. C. Feldman, R. L. Kaufman, P. J. Silverman, and R. A. Zuhr, Phys. Rev. Lett. 39, 38 (1977).
[34]D. D. Koelling, A. J. Freeman, and F. M. Mueller, Phys. Rev. B 1, 1318 (1970); D. D. Koelling, Phys. Rev. 188, 1049 (1969).
[35]P. Hohenberg and W. Kohn, Phys. Rev. 136, B864 (1964); W. Kohn and L. J. Sham, Phys. Rev. 140, A1133 (1965); 145, 561 (1966).
[36]For the corrected form of Wigner's original formula see D. Pines, *Elementary Excitations in Solids* (Benjamin, New York, 1963), Eq. (3.58).
[37]D. D. Koelling and B. N. Harmon, J. Phys. C 10, 3107 (1977).
[38]S. L. Cunningham, Phys. Rev. B 10, 4988 (1974).
[39]O. Jepsen and O. K. Andersen, Solid State Commun. 9, 1763 (1971); G. Lehman and M. Taut, Phys. Status Solidi 54, 468 (1972).
[40]E. Caruthers and L. Kleinman, Phys. Rev. Lett. 35, 738 (1975).
[41]H. Krakauer, M. Posternak, and A. J. Freeman, Phys. Rev. Lett. 43, 1885 (1979).
[42]K. Yonehara and L. D. Schmidt, Surf. Sci. 25, 238 (1971); T. E. Felter, R. A. Barker, and P. J. Estrup, Phys. Rev. Lett. 38, 1138 (1977); M. K. Debe and D. A. King, J. Phys. C 10, L303 (1977); I. Stensgaard, L. C. Feldman, and P. J. Silverman, Phys. Rev. Lett. 42, 247 (1979); A. J. Melmed, R. T. Tung, W. R. Graham, and G.D.W. Smith, Phys. Rev. Lett. 43, 1521 (1979). Also see references therein.
[43]E. Tosatti, Solid State Commun. 25, 637 (1978).
[44]T. M. Duc, C. Guillot, Y. Lassailly, J. Lecante, Y. Jughet, and J. C. Vedrine, Phys. Rev. Lett. 43, 789 (1979).
[45]P. J. Citrin, G. K. Wertheim, and Y. Baer, Phys. Rev. Lett. 41, 1425 (1978). Also see Refs. 2 and 3.
[46]B. A. Barker and P. J. Estrup, Phys. Rev. Lett. 41, 1307 (1978).
[47]See Stensgaard *et al.* in Ref. 42.
[48]N. Elyashar and D. Koelling, Phys. Rev. B 13, 5362 (1976).
[49]J. A. Appelbaum and D. R. Hamann, Phys. Rev. B 6, 2166 (1972)

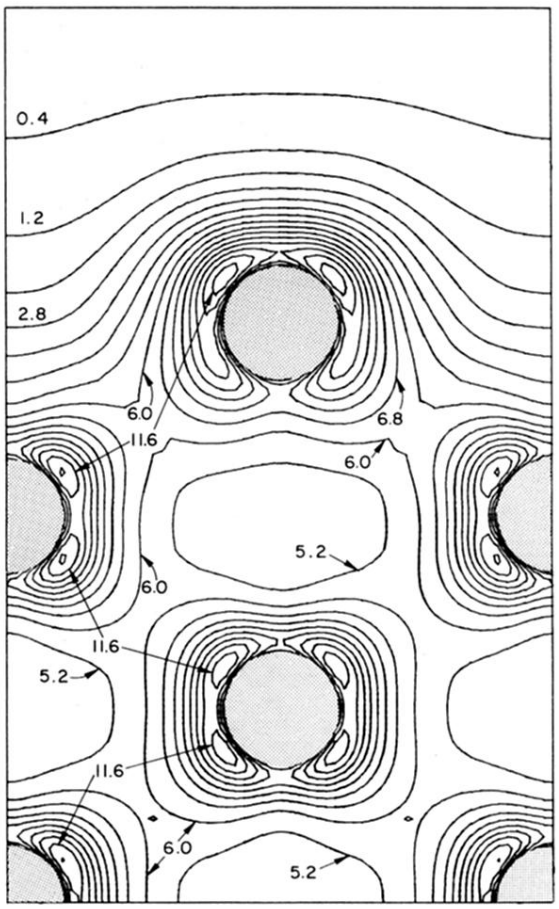

FIG. 3. Contour plot of the total valence charge density. Successive contours are separated by 0.8 in units of electrons per bulk unit cell.